Article

Nitrosyl Derivatives of Diiron(I) Dithiolates Mimic the Structure and Lewis Acidity of the [FeFe]-Hydrogenase Active Site

Matthew T. Olsen, Maurizio Bruschi, Luca De Gioia, Thomas B. Rauchfuss, and Scott R. Wilson

J. Am. Chem. Soc., **2008**, 130 (36), 12021-12030 • DOI: 10.1021/ja802268p • Publication Date (Web): 14 August 2008

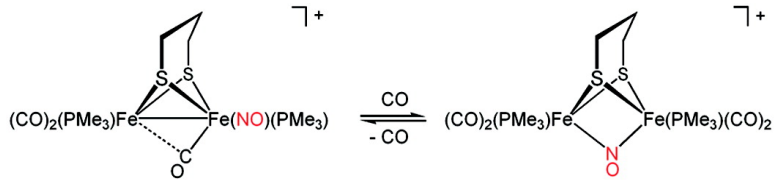

More About This Article

Additional resources and features associated with this article are available within the HTML version:

- Supporting Information
- Links to the 1 articles that cite this article, as of the time of this article download
- Access to high resolution figures
- Links to articles and content related to this article
- Copyright permission to reproduce figures and/or text from this article

View the Full Text HTML

J|A|C|S
ARTICLES

Published on Web 08/14/2008

Nitrosyl Derivatives of Diiron(I) Dithiolates Mimic the Structure and Lewis Acidity of the [FeFe]-Hydrogenase Active Site

Matthew T. Olsen,[†] Maurizio Bruschi,[‡] Luca De Gioia,*[,‡] Thomas B. Rauchfuss,*[,†] and Scott R. Wilson[†]

Department of Chemistry, University of Illinois at Urbana-Champaign, Urbana, Illinois 61801, and Department of Biotechnology and Biosciences, University of Milano—Bicocca, Piazza della Scienza 1, 20126 Milan, Italy

Received March 31, 2008; E-mail: rauchfuz@uiuc.edu; luca.degioia@unimib.it

Abstract: This study probes the impact of electronic asymmetry of diiron(I) dithiolato carbonyls. Treatment of $Fe_2(S_2C_nH_{2n})(CO)_{6-x}(PMe_3)_x$ compounds ($n = 2, 3$; $x = 1, 2, 3$) with $NOBF_4$ gave the derivatives $[Fe_2(S_2C_nH_{2n})(CO)_{5-x}(PMe_3)_x(NO)]BF_4$, which are electronically unsymmetrical because of the presence of a single NO^+ ligand. Whereas the monophosphine derivative is largely undistorted, the bis(PMe_3) derivatives are distorted such that the CO ligand on the $Fe(CO)(PMe_3)(NO)^+$ subunit is semibridging. Two isomers of $[Fe_2(S_2C_3H_6)(CO)_3(PMe_3)_2(NO)]BF_4$ were characterized spectroscopically and crystallographically. Each isomer features electron-rich $Fe(CO)_2PMe_3$ and electrophilic $Fe(CO)(PMe_3)(NO)^+$ subunits. These species are in equilibrium with an unobserved isomer that reversibly binds CO ($\Delta H = -35$ kJ/mol, $\Delta S = -139$ J mol^{-1} K^{-1}) to give the symmetrical adduct $[Fe_2(S_2C_3H_6)(\mu\text{-NO})(CO)_4(PMe_3)_2]BF_4$. In contrast to $Fe_2(S_2C_3H_6)(CO)_4(PMe_3)_2$, the bis($PMe_3$) nitrosyl complexes readily undergo CO substitution to give the $(PMe_3)_3$ derivatives. The nitrosyl complexes reduce at potentials that are ~1 V milder than their carbonyl counterparts. Results of density functional theory calculations, specifically natural bond orbital analysis, reinforce the electronic resemblance of the nitrosyl complexes to the corresponding mixed-valence diiron complexes. Unlike other diiron dithiolato carbonyls, these species undergo reversible reductions at mild potentials. The results show that the novel structural and chemical features associated with mixed-valence diiron dithiolates (the so-called H_{ox} models) can be replicated in the absence of mixed-valency by the introduction of electronic asymmetry.

Introduction

Modeling of the hydrogenase enzymes complements biophysical studies, providing insights into the mechanism and spectroscopy relevant to this important family of biocatalysts.[1,2] The [FeFe]-hydrogenases are particularly attractive for modeling studies because the $Fe_2(SR)_2(CO)_{6-x}L_x$ core resembles well-known organoiron complexes that are easily assembled with a variety of ligands and thiolates.[3,4] Variation of the coligands L and the thiolate SR offers the prospect of tuning the redox potentials and basicity of this diiron center. These variations in turn can affect the catalytic properties of the diiron center, which undergoes three characteristic reactions: reversible binding of CO, 1-electron redox, and catalytic interconversion of protons and dihydrogen. Although hundreds of derivatives of $Fe_2(SR)_2(CO)_{6-x}L_x$ have been studied as models for the [FeFe]-hydrogenases, no $(Fe^I)_2$ compound examined to date exhibits the single most distinctive structural feature of the enzyme: the "rotated" nature of the distal iron center (Scheme 1). Previously we reported a method for inducing rotation that requires strong Lewis acids and a highly basic diiron center, but resulting species were thermally unstable.[5]

Scheme 1. Structure of the Diiron Active Site of [FeFe]-Hydrogenases (X = CH_2, NH, O)

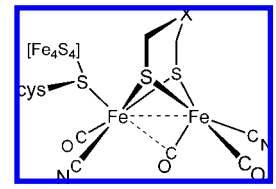

The rotated structure is observed for the two active states, as revealed by crystallographic studies of enzymes obtained from *Clostridium pasteurianum* and *Desulfovibrio desulfuricans*.[6] The rotated geometry contrasts with the idealized C_{2v} structure and has recently been replicated in models for the H_{ox} state, which feature a mixed-valence diiron core.[7,8] The geometry of the

[†] University of Illinois at Urbana-Champaign.
[‡] University of Milano—Bicocca.

(1) De Lacey, A. L.; Fernández, V. M.; Rousset, M.; Cammack, R. *Chem. Rev.* **2007**, *107*, 4304–4330.
(2) (a) Fontecilla-Camps, J. C.; Volbeda, A.; Cavazza, C.; Nicolet, Y. *Chem. Rev.* **2007**, *107*, 4273–4303. (b) Vignais, P. M.; Billoud, B. *Chem. Rev.* **2007**, *107*, 4206–4272.
(3) Liu, X.; Ibrahim, S. K.; Tard, C.; Pickett, C. J. *Coord. Chem. Rev.* **2005**, *249*, 1641–1652.
(4) Hogarth, G. In *Comprehensive Organometallic Chemistry III*; Crabtree, R., Mingos, M., Eds.; Elsevier: Amsterdam, 2007.
(5) Justice, A. K.; Zampella, G.; De Gioia, L.; Rauchfuss, T. B. *Chem. Commun.* **2007**, 2019–2021.

diiron site in the H_{red} state is unclear: it has either a rotated diiron(I) or diiron(II) core and a terminal hydride ligand.[9] From a mechanistic perspective, and relevant to understanding the hydrogenases as well as exploiting the diiron dithiolate platform for other applications, the rotated structure is of special significance because it provides a well-defined site for the binding of substrates.[1]

Many different types of ligands have been installed at one or more of the six terminal sites on the diiron dithiolate framework, including, in approximate order of their abundance, phosphines,[10] phosphites,[11] thioethers and bridging thiolates,[12,13] isocyanides,[14] carbenes,[15] arsines,[11] and alkenes.[16] Prior to this work, strong acceptor ligands had not been installed on the diiron(I) dithiolato platform, although electrophiles were found to add to the Fe−Fe bond.[17] In this work, we have examined the ability of NO^+ to alter the electronic structure of the diiron dithiolate carbonyls. As one of strongest acceptor ligands in inorganic chemistry,[18] NO^+ often forms complexes that are isoelectronic and isostructural with CO compounds. We show in this work, however, that NO^+ forms diiron dithiolates that are *not* isostructural with the corresponding carbonyl complexes and that these nitrosyl complexes display enhanced Lewis acidity. Although iron nitrosyl thiolates have attracted intense interest,[19] the derivatives described below are novel. Closest to the present complexes are the Roussin esters $Fe_2(SR)_2(NO)_4$,[20] but substituted derivatives of these spin-paired 34-electron diiron complexes have not been well-developed.[21]

Results

Synthesis of $[Fe_2(S_2C_nH_{2n})(CO)_{5-x}(PMe_3)_x(NO)]BF_4$. When $NOBF_4$ was employed as a NO^+ source, PMe_3-substituted diiron dithiolato carbonyls were found to readily undergo nitrosylation to afford monosubstituted products in good yields (eq 1). Thus, CH_2Cl_2 solutions of the complexes $Fe_2(S_2C_nH_{2n})(CO)_{6-x}(PMe_3)_x$ ($x = 1, 2$) were found to react efficiently with suspensions of $NOBF_4$ over the course of hours at 0 °C. In this way, we prepared $[Fe_2(S_2C_nH_{2n})(CO)_4(PMe_3)(NO)]BF_4$ for $n = 2$ (**1**) and 3 (**1′**) and $[Fe_2(S_2C_nH_{2n})(CO)_3(PMe_3)_2(NO)]BF_4$ for $n = 2$ (**2**) and 3 (**2′**) (eq 1). The IR spectra of **1** and **2** displayed ν_{CO} bands that were ~50 cm^{-1} higher in energy than those of their precursors. Each displayed a strong ν_{NO} band in the range ~1825−1760 cm^{-1}.

$$Fe_2(S_2C_nH_{2n})(CO)_{6-x}(PMe_3)_x + NOBF_4 \rightarrow [Fe_2(S_2C_nH_{2n})(CO)_{5-x}(PMe_3)_x(NO)]BF_4 + CO \quad (1)$$

Solutions of the mono- and diphosphines decompose over the course of hours at room temperature; the diphosphines slowly convert to mixtures containing the trisphosphine derivatives $[Fe_2(S_2C_nH_{2n})(CO)_2(PMe_3)_3(NO)]BF_4$ (see below) as well as other unidentified species.

Crystallographic Results. The structures **1**, **2**, **2′**, and $[Fe_2(S_2C_3H_6)(CO)_2(PMe_3)_3(NO)]BF_4$ (**3′**) were verified crystallographically. As expected, the $(Fe^I)_2(SR)_2$ core is complemented by six terminal ligands.[22] The iron−ligand distances in **1**, **2**, **2′**, and **3′** are unremarkable, and the carbonyl and nitrosyl ligands were distinguished by the Fe−NO distances, which were observed to be ~0.15 Å shorter than the Fe−CO distances (Figures 1−3).

The striking aspect of these structures is the distortion of the Fe_2L_6 framework from the usual[4] eclipsed quasi-C_{2v} geometry (Scheme 2). Especially for **2** and **2′**, the $Fe(CO)(PMe_3)(NO)^+$ subunit is rotated to orient a CO ligand into a semibridging position. This distortion is manifested in a more acute $Fe^{CO}-Fe^{NO}-CO$ bond angle (Ψ), where Fe^{CO} and Fe^{NO} refer to the NO-free and NO-bearing iron atoms, respectively. Whereas mixed-valence diiron (I/II) dithiolato carbonyls display semibridging carbonyls with $\Psi < 80°$ (see Table 1), for diiron(I) dithiolato carbonyls, Ψ falls within the narrow range 95−105° [e.g., for $Fe_2(S_2C_3H_6)(CO)_4(PMe_3)_2$, $\Psi = 103.6°$].[23] For previously reported (NO^+-free) diiron dithiolates, this value varies only slightly (±5°), depending on the size and chelating nature of the other ligands (see Table 1). Previously reported unsymmetrically substituted derivatives usually feature unremarkable structures.[24,25] One exception is the triphos complex.[22] Because

(6) (a) Nicolet, Y.; Lemon, B. J.; Fontecilla-Camps, J. C.; Peters, J. W. *Trends Biochem. Sci.* **2000**, *25*, 138–143. (b) Pandey, A. S.; Harris, T. V.; Giles, L. J.; Peters, J. W.; Szilagyi, R. K. *J. Am. Chem. Soc.* **2008**, *130*, 4533–4540.
(7) Justice, A. K.; Rauchfuss, T. B.; Wilson, S. R. *Angew. Chem., Int. Ed.* **2007**, *46*, 6152–6154.
(8) Liu, T.; Darensbourg, M. Y. *J. Am. Chem. Soc.* **2007**, *129*, 7008–7009.
(9) van der Vlugt, J. I.; Rauchfuss, T. B.; Whaley, C. M.; Wilson, S. R. *J. Am. Chem. Soc.* **2005**, *127*, 16012–16013.
(10) Arabi, M. S.; Mathieu, R.; Poilblanc, R. *J. Organomet. Chem.* **1979**, *177*, 199–209.
(11) de Beer, J. A.; Haines, R. J. *J. Organomet. Chem.* **1972**, *36*, 297–312.
(12) Song, L.-C.; Yang, Z.-Y.; Bian, H.-Z.; Hu, Q.-M. *Organometallics* **2004**, *23*, 3082–3084.
(13) Tard, C.; Liu, X.; Ibrahim, S. K.; Bruschi, M.; De Gioia, L.; Davies, S. C.; Yang, X.; Wang, L.-S.; Sawers, G.; Pickett, C. J. *Nature* **2005**, *433*, 610–614.
(14) (a) Nehring, J. L.; Heinekey, D. M. *Inorg. Chem.* **2003**, *42*, 4288–4292. (b) Boyke, C. A.; Rauchfuss, T. B.; Wilson, S. R.; Rohmer, M.-M.; Bénard, M. *J. Am. Chem. Soc.* **2004**, *126*, 15151–15160.
(15) (a) Capon, J.-F.; El Hassnaoui, S.; Gloaguen, F.; Schollhammer, P.; Talarmin, J. *Organometallics* **2005**, *24*, 2020–2022. (b) Tye, J. W.; Lee, J.; Wang, H. W.; Mejia-Rodriguez, R.; Reibenspies, J. H.; Hall, M. B.; Darensbourg, M. Y. *Inorg. Chem.* **2005**, *44*, 5550–5552.
(16) Lawrence, J. D.; Li, H.; Rauchfuss, T. B. *Chem. Commun.* **2001**, 1482–1483.
(17) (a) Arabi, M. S.; Mathieu, R.; Poilblanc, R. *Inorg. Chim. Acta* **1977**, *23*, L17–L18. (b) Arabi, M. S.; Mathieu, R.; Poilblanc, R. *Inorg. Chim. Acta* **1979**, *34*, L207–L208. (c) Bonnet, J. J.; Mathieu, R.; Poilblanc, R.; Ibers, J. A. *J. Am. Chem. Soc.* **1979**, *101*, 7487–7496.
(18) (a) Mitoraj, M.; Michalak, A. *Organometallics* **2007**, *26*, 6576–6580. (b) Richter-Addo, G. B.; Legzdins, P. *Metal Nitrosyls*; Oxford University Press: New York, 1992. (c) Wu, C.-Y.; Chen, L.-H.; Hwang, W.-S.; Chen, H.-S.; Hung, C.-H. *J. Organomet. Chem.* **2004**, *689*, 2192–2200.
(19) (a) Butler, A. R.; Megson, I. L. *Chem. Rev.* **2002**, *102*, 1155–1165. (b) Wasser, I. M.; de Vries, S.; Moënne-Loccoz, P.; Schröder, I.; Karlin, K. D. *Chem. Rev.* **2002**, *102*, 1201–1234. (c) Tsai, M.-L.; Liaw, W.-F. *Inorg. Chem.* **2006**, *45*, 6583–6585. (d) Conradie, J.; Quarless, D. A., Jr.; Hsu, H.-F.; Harrop, T. C.; Lippard, S. J.; Koch, S. A.; Ghosh, A. *J. Am. Chem. Soc.* **2007**, *129*, 10446–10456. (e) Harrop, T. C.; Song, D.; Lippard, S. J. *J. Am. Chem. Soc.* **2006**, *128*, 3528–3529. (f) Harrop, T. C.; Song, D.; Lippard, S. J. *J. Inorg. Biochem.* **2007**, *101*, 1730–1738.
(20) (a) Rauchfuss, T. B.; Weatherill, T. D. *Inorg. Chem.* **1982**, *21*, 827–831. (b) Conrado, C. L.; Bourassa, J. L.; Egler, C.; Wecksler, S.; Ford, P. C. *Inorg. Chem.* **2003**, *42*, 2288–2293.
(21) (a) Chen, H.-W.; Lin, C.-W.; Chen, C.-C.; Yang, L.-B.; Chiang, M.-H.; Liaw, W.-F. *Inorg. Chem.* **2005**, *44*, 3226–3232. (b) Lee, C.-M.; Chen, C.-H.; Chen, H.-W.; Hsu, J.-L.; Lee, G.-H.; Liaw, W.-F. *Inorg. Chem.* **2005**, *44*, 6670–6679.
(22) Adam, F. I.; Hogarth, G.; Richards, I.; Sanchez, B. E. *Dalton Trans.* **2007**, 2495–2498.
(23) Zhao, X.; Georgakaki, I. P.; Miller, M. L.; Yarbrough, J. C.; Darensbourg, M. Y. *J. Am. Chem. Soc.* **2001**, *123*, 9710–9711.
(24) Duan, L. L.; Wang, M.; Li, P.; Na, Y.; Wang, N.; Sun, L. C. *Dalton Trans.* **2007**, 1277–1283.
(25) Justice, A. K.; Zampella, G.; De Gioia, L.; Rauchfuss, T. B.; van der Vlugt, J. I.; Wilson, S. R. *Inorg. Chem.* **2007**, *46*, 1655–1664.

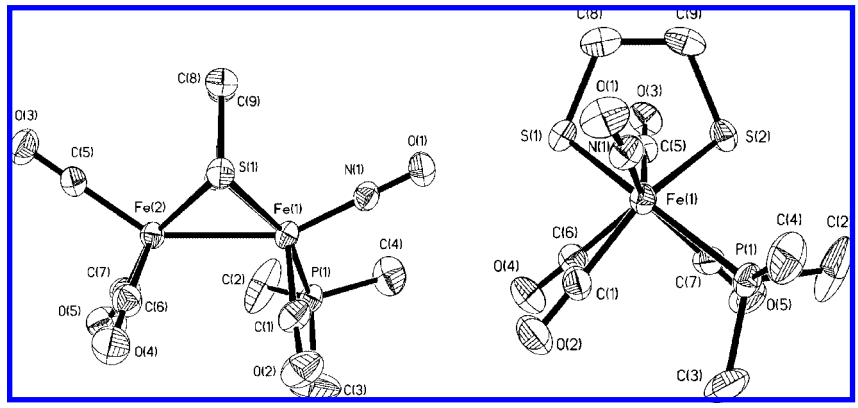

Figure 1. Structure of **1** with thermal ellipsoids set at 35%: (left) side view; (right) end view. Disordered anions and hydrogen atoms have been omitted for clarity. Key bond distances (Å): Fe1−Fe2, 2.5529(9); Fe1−N1, 1.669(4); Fe1−P1, 2.2971(13); Fe1−C1, 1.821(5); Fe2−C5, 1.804(4); Fe2−C6, 1.804(5); Fe2−C7: 1.794(5).

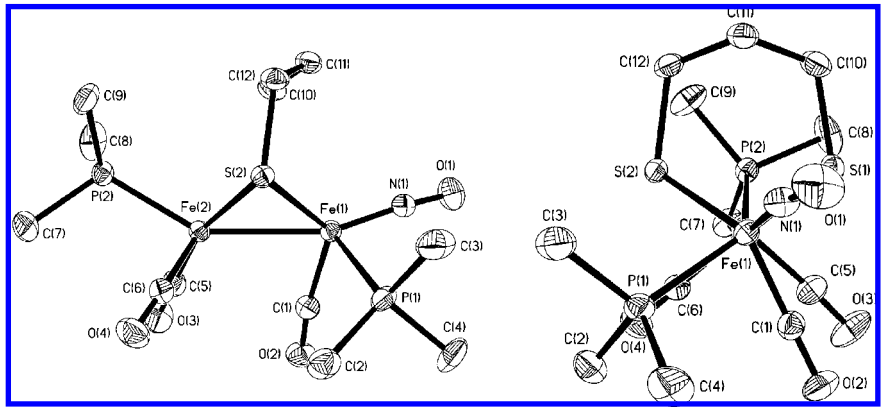

Figure 2. Structure of $\mathbf{2'^{ap}}$ with thermal ellipsoids set at 35%: (left) side view; (right) end view. Hydrogen atoms, disordered methyl groups on P2, the anion, and solvate have been omitted for clarity. Key bond distances (Å): Fe1−Fe2, 2.5806(5); Fe1−N1, 1.648(3); Fe1−P1, 2.2622(8); Fe1−C1, 1.794(3); Fe2−C5, 1.778(3); Fe2−C6, 1.777(3); Fe2−P2, 2.2231(8); Fe2−C1, 2.767(3).

Scheme 2. Idealized Frameworks for (left) the C_{2v} Structure (Fe−CO Vectors Twisted for Clarity) and (right) the T-Shaped Rotated Framework

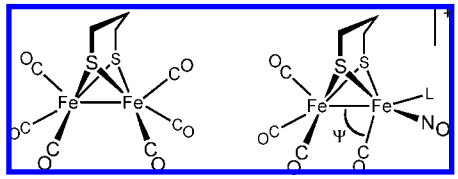

of its rotated nature, the $Fe(CO)(PMe_3)(NO)^+$ center adopts an approximately T-shaped orientation.

Compound **1** crystallized with two molecules in its asymmetric unit, both having a Ψ value of ∼91° (Figure 1). These are less than the typical value (∼100°) but by the definition of Crabtree[26] correspond to terminal carbonyls. Otherwise, the structure is not unusual: the ligands are eclipsed and the $Fe(CO)_3$ subunit is unaffected.

Two separate rotamers of the bisphosphine propanedithiolate **2′** crystallized. Each is severely distorted. For one rotamer, labeled $\mathbf{2'^{ap}}$, the phosphine on the $Fe(CO)_2(PMe_3)$ center occupies an apical site, and Ψ = 76° (Figure 2).

Table 1. Fe−Fe−CO Bond Angles (Ψ) for Various Diiron Dithiolate Compounds

compound	Ψ (deg)[a]
1	91.3, 91.1
2	80.5
$\mathbf{2'^{ap}}$	76.1
$\mathbf{2'^{ba}}$	62.1, 66.6
$[Fe_2(S_2C_3H_6)(CO)_3(dppv)(PMe_3)]^+$ [b]	72.0
$[Fe_2(S_2C_3H_4)(CO)_4(iMes)(PMe_3)]^+$ [c]	56.8
$Fe_2(S_2C_3H_6)(CO)_6$ [d]	101.0
$Fe_2(S_2C_3H_6)(CO)_5(P(C_6H_5)_3)$ [e]	96.2
$Fe_2(S_2C_3H_6)(CO)_4(PMe_3)_2$	103.6
$Fe_2(S_2C_3H_6)(CO)_3(triphos)$ [f]	88.3

[a] The smallest Ψ value among those for the various carbonyls is reported; two values are given for compounds having two molecules in the asymmetric unit. [b] From ref 7; dppv is *cis*-1,2-bis(diphenylphosphino)-ethene. [c] From ref 8; iMes is *N,N′*-bis(mesityl)imidazolidene. [d] From ref 27. [e] From ref 28. [f] From ref 29; triphos is (κ^3-$Ph_2P(CH_2)_2P(Ph)(CH_2)_2PPh_2$).

In the second rotamer, $\mathbf{2'^{ba}}$, the phosphine ligand on the $Fe(CO)_2(PMe_3)$ center is basal, and the $Fe(CO)(PMe_3)(NO)^+$ center is even more distorted than that in $\mathbf{2'^{ap}}$. The shift of the PMe_3 ligand from the apical to the basal site on the $Fe(CO)_2PMe_3$ center moves the bridging CO ligand into a more symmetrical position. Two molecules were found in the asymmetric unit, with Ψ values of ∼62 and 67°, i.e., these molecules contain bent semibridging carbonyls (Figure 3). The two distinct structures of $\mathbf{2'^{ba}}$ indicate some flexibility for the semibridging carbonyl parallel to the Fe−Fe vector. Because of the increased

(26) Crabtree, R. H.; Lavin, M. *Inorg. Chem.* **1986**, *25*, 805–812.
(27) Lyon, E. J.; Georgakaki, I. P.; Reibenspies, J. H.; Darensbourg, M. Y. *Angew. Chem., Int. Ed.* **1999**, *38*, 3178–3180.
(28) Li, P.; Wang, M.; He, C.; Li, G.; Liu, X.; Chen, C.; Åkermark, B.; Sun, L. *Eur. J. Inorg. Chem.* **2005**, 2506–2513.

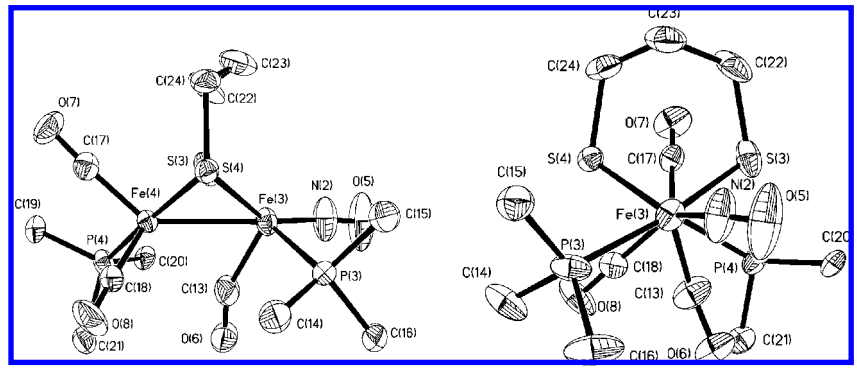

Figure 3. Structure of **2′ba** with thermal ellipsoids set at 35%: (left) side view; (right) end view. Of the two molecules in the asymmetric unit, the one with the smaller Ψ value (62.1°) is displayed. Hydrogen atoms, disordered methyl groups on P4, disorder in C13 and O6, the anion, and solvate have been omitted for clarity. Key bond distances (Å): Fe3−Fe4, 2.5433(12); Fe3−N2, 1.616(6); Fe3−P3, 2.253(2); Fe3−C13, 1.778(9); Fe4−C13, 2.323(9); Fe4−C17, 1.747(7); Fe4−C18, 1.786(7); Fe4−P4, 2.273(4).

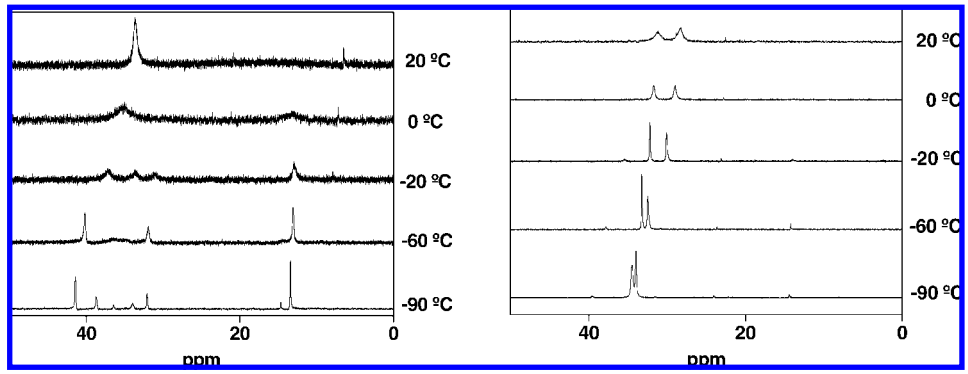

Figure 4. 202 MHz ^{31}P NMR spectra of (left) **2′** and (right) **2** at various temperatures (CD_2Cl_2 solutions).

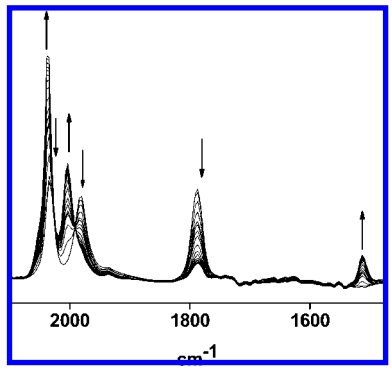

Figure 5. IR spectra recorded at intervals over the course of 10 min for the carbonylation of **2′** (CH_2Cl_2 solution, −80 °C). Note the diminution of the 1797 cm^{-1} band for **2′** and the concomitant appearance of the band at 1513 cm^{-1}, assigned to $\nu_{\mu\text{-NO}}$ in **2′**CO.

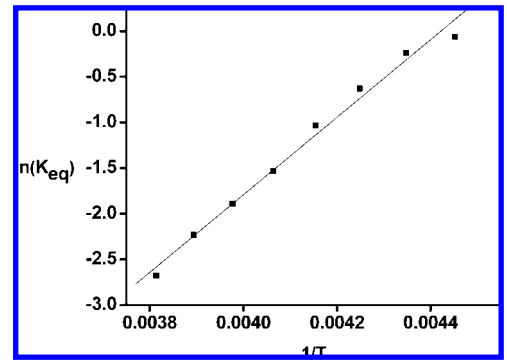

Figure 6. Plot of ln(K_{eq}) vs 1/T for 0.022 M **2′** in CH_2Cl_2 under a CO pressure of 1 atm.

rotation of the $[Fe(CO)(PMe_3)(NO)]^+$ subunit (compared with that seen in **2′ap**), the vacant coordination site on Fe^{NO} is particularly open and more closely resembles the diiron coordination environment in the H_{ox} state and models thereof.[7,8] Although semibridging carbonyls are present in the solid state, a band for $\nu_{\mu\text{-CO}}$ is not apparent in the solution IR spectra of bulk samples of **2′** because **2′ba** is a minority component. However, a $\nu_{\mu\text{-CO}}$ band is observed in the solid-state IR spectrum of single crystals of **2′**.

The framework of ethanedithiolate **2** resembles that for **2′ap** (see the Supporting Information). Only a single isomer was observed in both the solid state and solution. The Ψ value (∼80°) is somewhat larger than for the propanedithiolate (i.e., FeCO is less bent), consistent with the expected diminished steric influence of the smaller dithiolate.[5]

Because two rotamers of **2′** crystallized, questions arose about the possibility that either **2′ap** or **2′ba** could be exceptional crystals that are not significantly represented in bulk samples. This issue was addressed through powder X-ray diffraction studies. Powder diffraction patterns for **2′ap** and **2′ba** were calculated from the single-crystal data. The powder diffraction data for bulk samples were shown to consist of these two isomers as well as a third component. **2′ap** was found to be the majority component, although calculations (see below) suggest that **2′ba** is ∼3 kcal/mol lower in energy. The third component corresponds to one or more species obtained when single-crystalline **2′** desolvates. The main point, however, is that **2′ap** and **2′ba** are significant components of the solid mixture and are not statistical outliers.

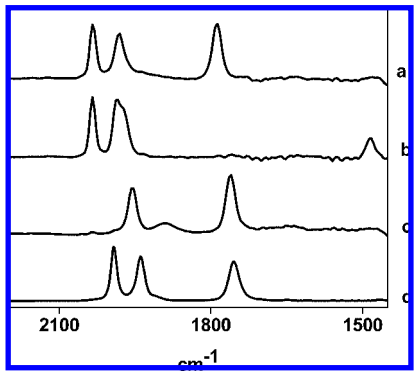

Figure 7. IR spectra of **2′** (CH_2Cl_2 solution) (a) at −78 °C, (b) following the addition of 1 equiv of PMe_3, (c) upon warming to −45 °C for 10 min, and (d) upon warming to room temperature for 3 h. For peak maxima, see the Experimental Section.

Table 2. Reduction Potentials (V) of **1**, **1′**, **2**, **2′** and Related Non-Nitrosylated Derivatives[a]

complex	$E_{1/2}$	$E_{1/2}$
$[Fe_2(S_2C_2H_4)(CO)_4(PMe_3)(NO)]^+$	−0.45[b]	−0.95[b]
$[Fe_2(S_2C_3H_6)(CO)_4(PMe_3)(NO)]^+$	−0.36	−1.03
$Fe_2(S_2C_3H_6)(CO)_5(PMe_3)$[c,d]	−1.86	–
$[Fe_2(S_2C_2H_4)(CO)_3(PMe_3)_2(NO)]^+$	−0.67	−0.98
$[Fe_2(S_2C_3H_6)(CO)_3(PMe_3)_2(NO)]^+$	−0.64	−0.98
$Fe_2(S_2C_3H_6)(CO)_4(PMe_3)_2$[c]	−2.08	–

[a] Conditions: 1.5 mM in CH_2Cl_2 with 100 mM Bu_4NPF_6 at 20 °C, unless otherwise specified, referenced vs Ag|AgCl (saturated KCl). [b] 0 °C. [c] In CH_3CN solution.[37] [d] Referenced vs Ag|$AgNO_3$.[28]

Table 3. NBO Charges of **2′ap**, **2′ba**, $Fe_2(S_2C_3H_6)(CO)_4(PMe_3)_2$, and $[Fe_2(S_2C_3H_6)(CO)_4(PMe_3)_2]^+$ Computed at the RI-BP86/def-TZVP Level of Theory

complex	$Fe(CO)_2(PMe_3)$	other FeL_3^z ($z = 0$ or 1+)
2′ba	−0.22	0.03
2′ap	−0.19	0.03
$Fe_2(S_2C_3H_6)(CO)_4(PMe_3)_2$	−0.19 to −0.18[a]	−0.19 to −0.21[a]
$[Fe_2(S_2C_3H_6)(CO)_4(PMe_3)_2]^+$	−0.19 to −0.21[a]	−0.02 to −0.00[a]

[a] The range of values encompasses the results for different isomers (see Supporting Information).

Table 4. Vibrational Frequencies (cm^{-1}) and Relative Intensities for **2′ap** and **2′ba** Computed at the RI-BP86/def-TZVP Level of Theory

2′ap ν_{NO} and ν_{CO} (rel. int.)	**2′ba** ν_{NO} and ν_{CO} (rel. int.)	observed (CH_2Cl_2 soln)
1814 (843)	1817 (795)	1787
1975 (289)	1880 (418)	
1978 (490)	1988 (532)	1981
2030 (780)	2028 (559)	2033

Further phosphine substitution occurs at the Fe^{NO} subunit to yield **3′** (see the Supporting Information). Aside from a slightly distorted $Fe(PMe_3)_2(NO)^+$ subunit containing a $Fe^{CO}-Fe^{NO}-P$ bond angle of 96°, the structure is typical.

DNMR Studies. Variable-temperature dynamic NMR (DNMR) studies indicated that the propanedithiolate **2′** consists of two major isomers in solution, as anticipated from the crystallography. At 150 °C, the ^{31}P NMR spectrum consisted of two well-resolved singlets (see the Supporting Information). When the sample was cooled, these peaks significantly broadened and decoalesced into a total of four peaks. Coalescence occurred at 25 and 10 °C, corresponding to the interconversion of **2′ap** and **2′ba** with an estimated free energy of activation in the range 51−52 kJ/mol. Below −60 °C, further splitting due to the slow equilibration of the bridging propanedithiolate was observed, as seen for non-nitrosylated $Fe_2(S_2C_3H_6)(CO)_4(PMe_3)_2$.[30]

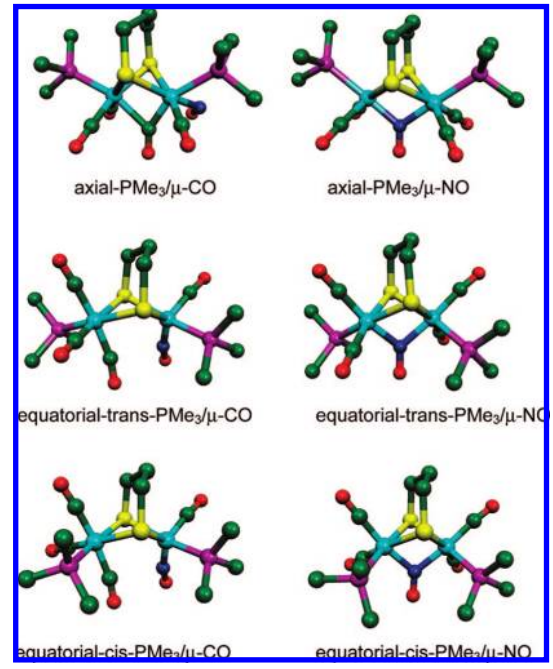

Figure 8. DFT-optimized structures of the possible isomers of **2′**CO. Atom color scheme: oxygen, red; nitrogen, blue; carbon, green; iron, cyan; sulfur, yellow; phosphorus, purple.

Table 5. Binding Energies (kcal/mol) for **2′ba** + CO → **2′**CO Computed at the RI-BP86/def-TZVP Level of Theory

reaction	ΔE
2′ba + CO → axial-PMe_3/μ-CO	23.4
2′ba + CO → axial-PMe_3/μ-NO	4.3
2′ba + CO → equatorial-cis-PMe_3/μ-CO	−0.3
2′ba + CO → equatorial-cis-PMe_3/μ-NO	−9.4
2′ba + CO → equatorial-trans-PMe_3/μ-CO	−1.6
2′ba + CO → equatorial-trans-PMe_3/μ-NO	−12.2

The ^{31}P NMR spectrum of the ethanedithiolate **2** displayed only two singlets over the temperature range from 20 to −90 °C (Figure 4). Thus, it appears that only the propanedithiolate exists as energetically distinct rotamers.

Carbonylation of $[Fe_2(S_2C_nH_{2n})(CO)_3(PMe_3)_2(NO)]^+$. Unlike other diiron(I) dithiolates, **2′** and **2** are Lewis acidic: both reversibly add CO at low temperatures. In the IR spectrum of the adduct **2′**CO, ν_{NO} absorbs at 1513 cm^{-1}, which is ∼200 cm^{-1} below the region for terminal nitrosyl ligands in this series. The spectra for the carbonylation process exhibit isosbestic behavior, indicative of an equilibrium between two principal species (see Figure 5). Compounds **1** and **1′** did not display similar behavior, but ^{31}P NMR indicated that **3′** also formed an adduct with CO at low temperatures (see the Supporting Information).

The IR spectra of **2′**CO are consistent with the presence of a bridging nitrosyl ligand. This assignment is supported by the low-temperature ^{31}P NMR spectrum, which indicated equivalent phosphine ligands. Both isomers of **2′** formed the same adduct.

(29) Hogarth, G.; Richards, I. *Inorg. Chem. Commun.* **2007**, *10*, 66–70.
(30) Georgakaki, I. P.; Thomson, L. M.; Lyon, E. J.; Hall, M. B.; Darensbourg, M. Y. *Coord. Chem. Rev.* **2003**, *238−239*, 255–266.

Scheme 3. Proposed Pathways for Carbonylation of **2′**

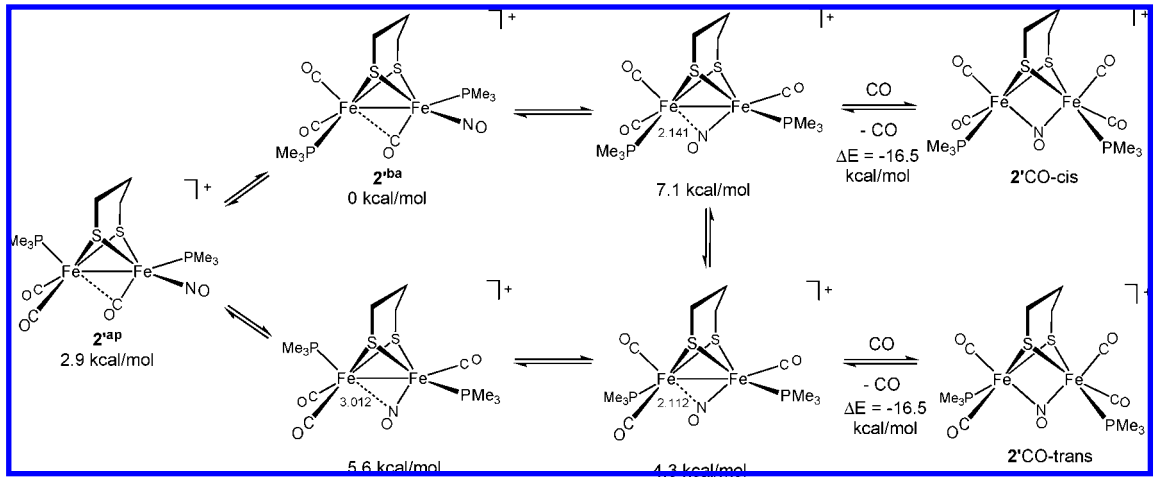

The 200 cm^{-1} shift of the ν_{NO} band, also predicted by density functional theory (DFT) calculations, is consistent with the relocation of the NO ligand from a terminal to a bridging position. Binding of CO by **2′** occurs with $\Delta H = -35$ kJ/mol and $\Delta S = -139$ J mol^{-1} K^{-1} (Figure 6), consistent with an associative process (eq 2):

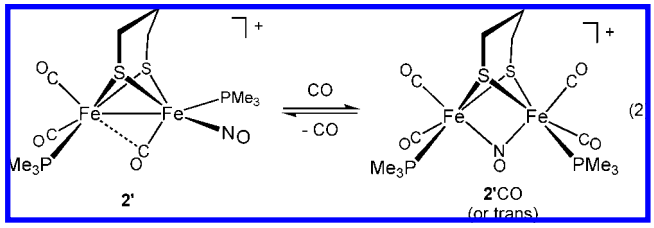

Despite the demonstrated affinity of **2′** for CO, solutions of **2′** did not appear to react with H_2. Furthermore, no H−D exchange was observed when solutions of **2′** and H_2 were treated with MeOD in the presence of noncoordinating base.

Like **2′**, ethanedithiolate **2** displays a similar affinity toward CO. In a competition study, a solution that was equimolar in **2** and **2′** was treated with 1 atm of CO. When the solution was cooled to −80 °C, both CO adducts were observed, but **2′**CO was favored by a factor of ∼7 relative to **2**CO. The adducts **2**CO and **2′**CO presumably occur as intermediates in the synthesis of **2′** from the reaction of NO^+ and $[Fe_2(S_2C_nH_{2n})CO)_4(PMe_3)_2$.

Labeling with ^{13}CO has proven to be an effective tool for probing the carbonylation of models for H_{ox} and H_{ox}^{CO},[31,32] but the present system is advantageous because the diamagnetism enabled analysis by ^{13}C NMR spectroscopy. Exposure of **2′** to ^{13}CO at −80 °C resulted primarily in a single isotopomer of **2′**CO and singly labeled **2′**. In **2′**^{13}CO, the label is proposed to be located at one of the two equivalent apical sites. The selectively labeled **2′** is proposed to arise by dissociation of ^{12}CO from one of these two equivalent apical sites. Upon thermal equilibration of the sample, the −80 °C spectrum displayed five ^{31}P-coupled doublets: two for **2′**CO and three for the major isomer of **2′** (see the Supporting Information).

When equimolar amounts of **1′** and **2′** were pressurized with ^{13}CO at −80 °C, the ^{31}P NMR spectra indicated carbonylation exclusively at **2′**, as expected since **1′** exhibits no Lewis acidity. Upon thermal equilibration, the ^{13}C NMR spectrum showed that **2′** alone was enriched. Similarly, when equimolar amounts of **2′** and **3′** were equilibrated under an atmosphere of ^{13}CO, enrichment was observed only at **2′**.

Reactions of PMe_3 with $[Fe_2(S_2C_nH_{2n})(CO)_3(PMe_3)_2(NO)]^+$. In contrast to the nucleophilicity of $Fe_2(S_2C_3H_6)(CO)_4(PMe_3)_2$, the nitrosyl compounds **2′** and **2** were found to be electrophilic. For example, **2′** is not visibly protonated by triflic acid, and **2′** and **2** react readily with PMe_3 to afford the corresponding trisphosphines $[Fe_2(S_2C_nH_{2n})(CO)_2(PMe_3)_3(NO)]BF_4$ (**3** and **3′**). Two intermediates for these conversions were detected by in situ IR spectroscopy. An initial adduct was observed immediately upon the addition of the phosphine to a CH_2Cl_2 solution of the diphosphine complex at −80 °C. IR spectra showed that ν_{NO} is most affected (Figure 7). The IR spectrum resembled that for the above-mentioned adducts **2′**CO and **2**CO, implicating the formation of a bridging NO complex. The ν_{NO} stretch is ∼25 cm^{-1} lower in energy.

The monophosphines **1** and **1′** were also found to readily undergo substitution by PMe_3 (to give **2** and **2′**, respectively) as well as by other nucleophiles (see the Supporting Information). In these cases, IR measurements suggested that the nucleophile initially adds to the $Fe(CO)_3$ subunit via a metastable intermediate containing a bridging CO, although this aspect was not pursued.

Electrochemistry. Each of the compounds **1**, **1′**, **2**, and **2′** exhibits two one-electron reduction steps (Table 2) but oxidizes only at very positive potentials (>1.3 V versus Ag|AgCl). For **1** and **1′**, the first reductions are reversible but the second reductions are reversible only at slow scan rates. Although $\Delta\nu_{NO}$ is much larger than $\Delta\nu_{CO}$, the effect of one-electron reduction is smaller than that seen for the one-electron reduction of mononuclear iron nitrosyls.[33] For **2′**, the first reduction is quasi-reversible ($i_{pa}/i_{pc} \approx 0.7$) at moderate scan rates (100 mV/s) and the second reduction is irreversible. The behavior of **2** is similar, although the first reduction is less reversible.

(31) Justice, A. K.; Nilges, M. J.; Rauchfuss, T. B.; Wilson, S. R.; De Gioia, L.; Zampella, G. *J. Am. Chem. Soc.* **2008**, *130*, 5293–5301.
(32) Thomas, C. M.; Liu, T.; Hall, M. B.; Darensbourg, M. Y. *Chem. Commun.* **2008**, 1563–1565.
(33) (a) Sellmann, D.; Blum, N.; Heinemann, F. W.; Hess, B. A. *Chem.—Eur. J.* **2001**, *7*, 1874–1880. (b) Serres, R. G.; Grapperhaus, C. A.; Bothe, E.; Bill, E.; Weyhermuller, T.; Neese, F.; Wieghardt, K. *J. Am. Chem. Soc.* **2004**, *126*, 5138–5153.

The reductions were determined to be one-electron processes by comparing their i_{pa} values with the i_{pc} value for the oxidation of $Fe_2(S_2C_3H_6)(CO)_4$(dppv), which is known to be a one-electron process.[34] Thus, in CH_2Cl_2 solution, compounds **1**−**3** are first reduced at the mild potentials of −0.36 (**1**) to −1.02 V (**3**) (potentials versus Ag|AgCl). Highlighting the electron-accepting character of these nitrosyl complexes, the potentials for the *second* reduction of the diphosphine derivatives **2** and **2′** are less negative than the *first* reduction step of the corresponding tetracarbonyl parent. Reduction of **1′** is ∼0.1 V milder than that of **1**, indicating the expected effect of the dithiolate bridge on the redox properties of the diiron derivatives.[5] In contrast to the behavior of compounds **1**, **1′**, **2**, and **2′**, related complexes lacking NO^+ display reversible *oxidations* and a single, poorly reversible reduction at highly negative potentials.[35,36]

DFT Calculations. DFT calculations accurately reproduced the experimental structure of **2′** (Figure S28 in the Supporting Information). The two isomers characterized by X-ray diffraction (**2′ba** and **2′ap**) correspond to the two most stable isomeric forms computed using DFT. However, several other isomers have energies within a few kcal/mol (see the Supporting Information). To quantitatively evaluate the effect of the NO^+ ligand on the electronic structures of **2′ap** and **2′ba**, natural bond orbital (NBO) charges (Table 3) were computed and compared to the corresponding values obtained for the optimized structure of the isoelectronic tetracarbonyl compound $Fe_2(S_2C_3H_6)(CO)_4(PMe_3)_2$. Related calculations for the oxidized species $[Fe_2(S_2C_3H_6)(CO)_4(PMe_3)_2]^+$ proved especially relevant. These species adopt "rotated" structures and are considered electronic models for the H_{ox} state of the active site.[34] Although absolute values of NBO charges must be interpreted cautiously,[38] it is evident that the charge densities on the Fe atoms are far from formal oxidation states, reflecting the covalent character of the complex. Most importantly, the NBO charges on the Fe atoms in **2′ba** and **2′ap**, which formally are Fe^IFe^I species, are more similar to the corresponding values calculated for the mixed-valence complex[7] $[Fe_2(S_2C_3H_6)(CO)_4(PMe_3)_2]^+$ than those in the subferrous $Fe_2(S_2C_3H_6)(CO)_4(PMe_3)_2$ species. In particular, it can be concluded that the Fe^{NO} atoms in **2′ba** and **2′ap** are electrophilic. This observation conforms with the experimentally characterized Lewis acidity of the **2′** complex (see above) and its structural dissimilarity to Fe^IFe^I diiron dithiolates.[7]

Computed IR bands for **2′ap** and **2′ba** are collected in Table 4. The calculations are consistent with **2′ap** being the major isomer in solution. Experimentally, signals corresponding to **2′ba** were not observed. Notably, the $\nu_{\mu\text{-CO}}$ band shifts by almost 100 cm^{-1} in moving from **2′ap** to **2′ba** as a result of the shortening of the C(O)−Fe^{CO} distance in **2′ba** (2.78 vs 2.33 Å). However, the computed C(O)−Fe^{CO} distance in **2′ba** could be underestimated because of the very flat potential energy surface corresponding to slight C(O)−Fe^{CO} distance modifications, as indicated also by the crystallographic results, which range from 2.33 to 2.47 Å. Calculations of the vibrational frequencies also support the assignment of the structure of **2′**CO (see above). For example, the μ-NO group was calculated to be 1522 cm^{-1}, which reasonably matches the experimental value of 1513 cm^{-1}.

In regard to the structure of **2′**CO, DFT calculations indicate that the symmetrical μ-NO-containing species is significantly more stable than the other isomers (Figure 8), in agreement with the experimental evidence. Previous computational results from Schaefer and co-workers[39] indicate a preference for structures with bridging NO as opposed to bridging CO in electron-rich late-transition-metal complexes. The reaction energy of the carbonylation for **2′ba**, −12.2 kcal/mol (Table 5), is also consistent with the experimental value.

Calculations predict that a high-energy species (axial-PMe_3/μ-CO; Figure 8 and Table 5) features PMe_3 groups in apical positions with a *bent* NO ligand (having an Fe−N−O angle of 123°). Interestingly, the Fe−Fe distance contracts to 2.591 Å. This in silico experiment demonstrates, in effect, the competition between bending of Fe−N−O and Fe−Fe bonding. In the other isomers, including the lowest-energy species, the Fe···Fe distances are nonbonding: 2.987 (apical-PMe_3/μ-CO), 3.342 (equatorial-PMe_3/μ-CO), and 2.968 Å (equatorial-PMe_3/μ-NO).

We were surprised to observe bridging nitrosyl ligands in the adducts **2**CO and **2′**CO because the precursor complexes featured a semibridging carbonyl poised to shift to the bridging position. Calculations indicate enhanced stability for the adducts with μ-NO ligands (Table 5). Two similar carbonylation pathways are possible, each beginning with a turnstile rotation of the FeNO(PMe_3)(CO) center (Scheme 3). The binding of CO directly to **2′ba** without prior turnstile rotation is unfavorable. Only one isomer of the CO adduct is observed experimentally.

Discussion

The starting complexes in this work, which are of the type $Fe_2(SR)_2(CO)_{6-x}L_x$, are well-known, having been well developed even in the 1970s.[40] Because diiron(I) dithiolato carbonyls are structurally similar to the active site of the [FeFe]-hydrogenases, hundreds of derivatives have been described in recent years.[4] Although slight deviations from idealized symmetry are encountered with bulky or constraining ligands (see Table 1), this paper describes the first derivatives where Fe^IFe^I structures deviate strongly from the well-established C_{2v} motif.[41,42] Our results demonstrate that electronic asymmetry imposed by ligands can cause very substantial geometric distortions otherwise induced by redox processes (Figure 9).[7,8] These distortions in turn impact reactivity and further indicate the versatility of the $Fe_2(SR)_2(CO)_{6-x}L_x$ platform.[4]

(34) Justice, A. K.; De Gioia, L.; Nilges, M. J.; Rauchfuss, T. B.; Wilson, S. R.; Zampella, G. *Inorg. Chem.* [Online early access]. DOI: 10.1021/ic8007552. Published Online: July 12, 2008.
(35) (a) Felton, G. A. N.; Vannucci, A. K.; Chen, J.; Lockett, L. T.; Okumura, N.; Petro, B. J.; Zakai, U. I.; Evans, D. H.; Glass, R. S.; Lichtenberger, D. L. *J. Am. Chem. Soc.* **2007**, *129*, 12521–12530. (b) Borg, S. J.; Behrsing, T.; Best, S. P.; Razavet, M.; Liu, X.; Pickett, C. J. *J. Am. Chem. Soc.* **2004**, *126*, 16988–16999. (c) Borg, S. J.; Tye, J. W.; Hall, M. B.; Best, S. P. *Inorg. Chem.* **2007**, *46*, 384–394.
(36) Gloaguen, F.; Lawrence, J. D.; Rauchfuss, T. B.; Bénard, M.; Rohmer, M.-M. *Inorg. Chem.* **2002**, *41*, 6573–6582.
(37) Mejia-Rodriguez, R.; Chong, D.; Reibenspies, J. H.; Soriaga, M. P.; Darensbourg, M. Y. *J. Am. Chem. Soc.* **2004**, *126*, 12004–12014.
(38) Reed, A. E.; Curtiss, L. A.; Weinhold, F. *Chem. Rev.* **1988**, *88*, 899–926.
(39) Wang, H.; Xie, Y.; King, R. B.; Schaefer, H. F., III *Inorg. Chem.* **2008**, *46*, 1836–1847.
(40) (a) Zhao, X.; Georgakaki, I. P.; Miller, M. L.; Mejia-Rodriguez, R.; Chiang, C.-Y.; Darensbourg, M. Y. *Inorg. Chem.* **2002**, *41*, 3917–3928. (b) Fauvel, K.; Mathieu, R.; Poilblanc, R. *Inorg. Chem.* **1976**, *15*, 976–978.
(41) Dahl, L. F.; Wei, C. H. *Inorg. Chem.* **1963**, *2*, 328–333.
(42) Winter, A.; Zsolnai, L.; Huttner, G. *Z. Naturforsch.* **1982**, *37b*, 1430–1436.
(43) Nicolet, Y.; Piras, C.; Legrand, P.; Hatchikian, C. E.; Fontecilla-Camps, J. C. *Structure* **1999**, *7*, 13–23.

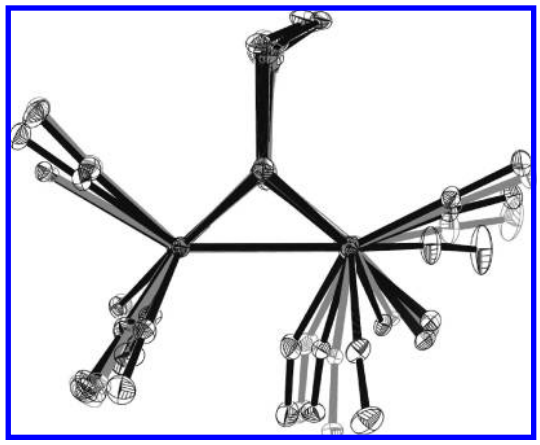

Figure 9. Overlay of (in order from left to right for the semibridging CO ligands): **2′^{ba}** (the examples in the asymmetric unit), **2′^{ap}**, **2**, and **1**. Thermal ellipsoids are set at 10%, and the anions, H atoms, and phosphine methyls have been omitted.

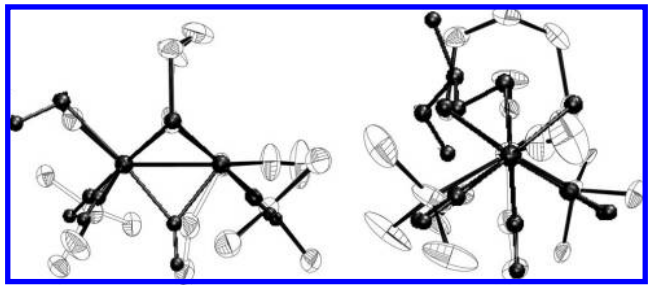

Figure 10. Overlay of **2′^{ba}** with the diiron portion of the H_{ox} state from *C. pasteurianum*.[45] The molecule of **2′^{ba}** with a smaller Ψ value was selected.

The electronic asymmetry is particularly acute in the diphosphines $[Fe_2(S_2C_nH_{2n})(CO)_3(PMe_3)_2(NO)]^+$, wherein the $Fe(CO)(PMe_3)(NO)^+$ center is electrophilic and the $Fe(CO)_2(PMe_3)$ center is electron-rich. As seen previously,[5] the positioning of the central methylene group on the propanedithiolate accentuates the asymmetry via nonbonding interactions with ligands occupying the apical sites. As also supported by DFT calculations, the new compounds approximate the structure of the H_{ox} state of the diiron site of the [FeFe]-hydrogenases (Figure 10), possibly because these compounds simulate the electronic asymmetry seen in H_{ox} and its models.[43] Not only do $[Fe_2(S_2C_nH_{2n})(CO)_x(PMe_3)_2(NO)]^+$ ($x = 3, 4$) resemble H_{ox}, but the binding of CO also gives a derivative that, like H_{ox}^{CO}, is symmetrized. It has been shown that binding of CO to valence-localized H_{ox} gives valence-delocalized H_{ox}^{CO}.[7,31,34,44] Unlike the H_{ox}/H_{ox}^{CO} system and its models, which interconvert 33- and 35-electron species, the 34-electron nitrosyl cations rearrange before forming the corresponding 36-electron adducts with CO.

In association with their novel structures, the new nitrosyl derivatives exhibit properties rarely seen in related complexes:
(1) *Lewis acidity*. Unlike the many previously reported 34-electron diiron(I) dithiolato complexes, the species $[Fe_2(S_2C_nH_{2n})(CO)_3(PMe_3)_2(NO)]^+$ are Lewis acidic.
(2) *Interconversions involving μ-NO ligands*. The binding of CO provides a rare example of the interconversion of terminal and bridging NO ligands. Relatively few examples of complexes with μ-NO ligands are known,[46] but for dimetallic mixed CO−NO complexes, NO bridges more often than CO.[39,47]
(3) *Mild reduction potentials*. Nitrosyl derivatives of the diiron(I) dithiolates reduce at potentials ∼1 V milder than those for related complexes.[48] For example, $Fe_2(S_2C_2H_4)(CO)_4(PMe_3)_2$ reduces at approximately −1.5 V versus Ag|AgCl, whereas the nitrosyl derivatives reduce at approximately −0.5 V. The effect of replacing CO by NO^+ is equivalent to protonation of the related CO derivative.[36,49]
(4) *Susceptibility toward ligand substitution*. Diiron(I) dithiolates resist polysubstitution by phosphine ligands, at least in the absence of chelate effects.[25,29] The presence of the nitrosyl ligand allows the preparation of $[Fe_2(S_2C_3H_6)(CO)_2(PMe_3)_3(NO)]^+$. This finding further establishes that the resistance of $Fe_2(S_2C_3H_6)(CO)_4(PMe_3)_2$ toward substitution is not due to steric factors but is the result of its diminished electrophilicity. The diiron centers in the enzymes are bound to *three* terminal donor ligands: two cyanides and one 4Fe−4S cluster.[13]
(5) *High rotational barriers*. The isolation of two rotamers separated by substantial (∼12 kcal/mol) barriers, as in the case of **2′^{ap}** and **2′^{ba}**, is unprecedented within the chemistry of diiron(I) dithiolato carbonyls. High barriers to isomerization are implicated for mixed-valence diiron dithiolates, which also feature semibridging CO ligands.[34] A "turnstile" mechanism[42,50] is assumed to describe the interconversion of **2′^{ap}** and **2′^{ba}** (Scheme 4).

Scheme 4. View Down the Fe−Fe Axis, Showing the Proposed Pathway for Interconversion of **2′^{ba}** and **2′^{ap}**

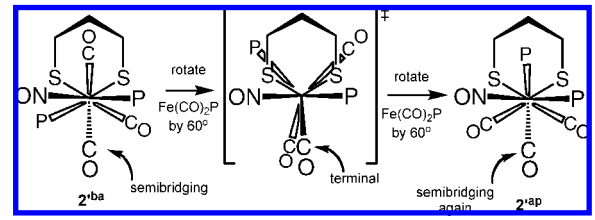

Experimental Section

Procedures and materials have recently been described elsewhere.[25] $NOBF_4$ was sublimed at 200 °C (0.02 mmHg).[51]

$[Fe_2(S_2C_2H_4)(CO)_4(PMe_3)(NO)]BF_4$, 1. At −30 °C, a mixture of 0.350 g (0.83 mmol) of $Fe_2(S_2C_2H_4)(CO)_5(PMe_3)$ and 0.095 g (0.81 mmol) of $NOBF_4$ in 20 mL of CH_2Cl_2 gave an intensely red solution over the course of 6 h. After the reaction mixture was concentrated to ∼2 mL, the product precipitated upon addition of ∼50 mL of hexanes followed by stirring for several minutes. The product was recrystallized by extraction into ∼2 mL of CH_2Cl_2 followed by the addition of 50 mL of hexanes. Yield: 0.303 g (72%). Layering of a CH_2Cl_2 solution of **1** with hexanes afforded red single crystals after several days at −30 °C. ^{1}H NMR (500 MHz, CD_2Cl_2): δ 3.23 (ddd, $J_{H-H} = 4.3$, 8.2, and 12.5 Hz, 1H, SCH_2), 3.07 (ddd, $J_{H-H} = 4.5$, 8.0, and 17.3 Hz, 1H, SCH_2), 2.94 (ddd, $J_{H-H} = 4.4$,

(44) Silakov, A.; Reijerse, E. J.; Albracht, S. P. J.; Hatchikian, E. C.; Lubitz, W. *J. Am. Chem. Soc.* **2007**, *129*, 11447–11458.
(45) Peters, J. W.; Lanzilotta, W. N.; Lemon, B. J.; Seefeldt, L. C. *Science* **1998**, *282*, 1853–1858.
(46) Paul, P. P.; Tyeklar, Z.; Farooq, A.; Karlin, K. D.; Liu, S.; Zubieta, J. *J. Am. Chem. Soc.* **1990**, *112*, 2430–2432.
(47) Hayton, T. W.; Legzdins, P.; Sharp, W. B. *Chem. Rev.* **2002**, *102*, 935–991.
(48) Cheah, M. H.; Borg, S. J.; Best, S. P. *Inorg. Chem.* **2007**, *46*, 1741–1750.
(49) Gloaguen, F.; Lawrence, J. D.; Rauchfuss, T. B. *J. Am. Chem. Soc.* **2001**, *123*, 9476–9477.
(50) (a) Adams, R. D.; Cotton, F. A.; Cullen, W. R.; Hunter, D. L.; Mihichuk, L. *Inorg. Chem.* **1975**, *14*, 1395–1399. (b) Lyon, E. J.; Georgakaki, I. P.; Reibenspies, J. H.; Darensbourg, M. Y. *J. Am. Chem. Soc.* **2001**, *123*, 3268–3278.

8.0, and 17.1 Hz, 1H, SCH_2), 2.88 (ddd, J_{H-H} = 4.4, 8.0, and 17.1 Hz, 1H, SCH_2), 1.85 (d, J_{P-H} = 11.6 Hz, 9H, PMe_3). ^{31}P NMR (202 MHz, CD_2Cl_2): (20 °C) δ 21.4 (s); (−75 °C) δ 23.3 (s). IR (CH_2Cl_2): ν_{CO} = 2091, 2042 cm^{-1}; ν_{NO} = 1824 cm^{-1}. ESI-MS: *m*/*z* 421.9 (M^+). Anal. Calcd (Found) for $C_9H_{13}BF_4Fe_2NO_5P_2S_2$: C, 21.25 (20.96); H, 2.49 (2.49); N, 2.75 (2.69).

[$Fe_2(S_2C_3H_6)(CO)_4(PMe_3)(NO)$]$BF_4$, 1′. This compound was prepared in the same way as **1**, starting from 0.189 g (0.36 mmol) of $Fe_2(S_2C_3H_6)(CO)_5(PMe_3)$ and 0.048 g (0.41 mmol) of $NOBF_4$. Yield: 0.131 g (58%). ^{1}H NMR (CD_2Cl_2): δ 2.72 (m, 2H, SCH_2), 2.56 (m, 2H, SCH_2), 2.15 (m, 1H, CH_2), 2.03 (m, 1H, CH_2), 1.84 (d, J_{P-H} = 11.4 Hz, 9H, PMe_3). ^{31}P NMR (CD_2Cl_2): (20 °C) δ 30.0 (s); (−80 °C) δ 32.3 (s), 24.9 (s). IR (CH_2Cl_2): ν_{CO} = 2089, 2036 cm^{-1}; ν_{NO} = 1813 cm^{-1}. ESI-MS: *m*/*z* 421.9 (M^+). Anal. Calcd (Found) for $C_9H_{13}BF_4Fe_2NO_5P_2S_2$: C, 22.97 (23.33); H, 2.89 (2.68); N, 2.68 (2.63).

[$Fe_2(S_2C_2H_4)(CO)_3(PMe_3)_2(NO)$]$BF_4$, 2. To a mixture of 0.400 g (0.85 mmol) of $Fe_2(S_2C_2H_4)(CO)_4(PMe_3)_2$ and 0.100 g (0.86 mmol) of $NOBF_4$ cooled to 0 °C was added 10 mL of CH_2Cl_2. After 3 h, the dark-brown-colored reaction mixture was concentrated in vacuo and precipitated upon addition of 50 mL of hexanes. Recrystallization from 1:6 CH_2Cl_2/hexane mixtures provided analytically pure product. Yield: 0.435 g (91%). Layering of a CH_2Cl_2 solution of the product with hexanes followed by cooling at −30 °C afforded deep-red single crystals. ^{1}H NMR (CD_2Cl_2): δ 2.98 (m, 2H, SCH_2), 2.82 (m, 1H, SCH_2), 2.74 (m, 1H, SCH_2), 1.75 (d, J_{P-H} = 11.2 Hz, 9H, PMe_3), 1.69 (d, J_{P-H} = 9.8 Hz, 9H, PMe_3). ^{31}P NMR (CD_2Cl_2): (20 °C) δ 31.2 (bs), 28.4 (bs); (−90 °C) δ 34.5 (s), 34.0 (s). IR (CH_2Cl_2): ν_{CO} = 2035, 1980 cm^{-1}; ν_{NO} = 1793 cm^{-1}. ESI-MS: *m*/*z* 470.1 (M^+). Anal. Calcd (Found) for $C_{11}H_{22}BF_4Fe_2NO_4P_2S_2$: C, 23.73 (23.78); H, 3.98 (4.26); N, 2.53 (2.54).

[$Fe_2(S_2C_3H_6)(CO)_3(PMe_3)_2(NO)$]$BF_4$, 2′. The preparation was modeled after that for **2** and used 0.504 g (1.05 mmol) of $Fe_2(S_2C_3H_6)(CO)_4(PMe_3)_2$ and 0.121 g (1.04 mmol) of $NOBF_4$. Yield: 0.382 g (64%). Layering of a CH_2Cl_2 solution of the product with hexanes followed by cooling to −30 °C afforded dark-brown needles. ^{1}H NMR (CD_2Cl_2): δ 2.58 (m, 2H, SCH_2), 2.45 (m, 2H, SCH_2), 1.10 (m, 2H, CH_2), 1.78 (d, J_{P-H} = 11.6 Hz, 9H, PMe_3), 1.72 (d, J_{P-H} = 10.1 Hz, 9H, PMe_3). ^{31}P NMR (CD_2Cl_2): (20 °C) δ 33.7 (bs), ∼19 (bs, v br); (−40 °C) δ 37.2 (s), 33.8 (s), 31.2 (s), 13.1 (s); (−90 °C) δ 41.4 (s), 38.7 (s), 36.4 (s), 34.0 (s), 32.0 (s), 14.6 (s), 13.4 (s). Integrations indicated that the δ 34.0 peak consisted of two overlapping signals. IR (CH_2Cl_2): ν_{CO} = 2033, 1981 cm^{-1}; ν_{NO} = 1787 cm^{-1}. ESI-MS: *m*/*z* 484.0 (M^+). Anal. Calcd (Found) for $C_{12}H_{24}BF_4Fe_2NO_4P_2S_2$: C, 25.25 (25.07); H, 4.24 (4.20); N, 2.45 (2.40).

[$Fe_2(S_2C_3H_6)(CO)_2(PMe_3)_3(NO)$]$BF_4$, 3′. To a solution of 0.141 g (0.25 mmol) of [$Fe_2(S_2C_3H_6)(CO)_3(PMe_3)_2(NO)$]$BF_4$ in 10 mL of CH_2Cl_2 cooled to −78 °C was added 1.27 mL of a 0.193 M solution of PMe_3 (0.25 mmol) in CH_2Cl_2. The solution was warmed to room termperature and maintained at that temperature until all of the intermediate ([$Fe_2(S_2C_3H_6)(\mu$-CO)$(CO)_2(PMe_3)_3(NO)$]BF_4) was converted to **3′** (∼ 2.5 h). The red product precipitated from solution upon addition of 50 mL of hexanes followed by removal of approximately $^1/_6$ of the total volume in vacuo. Yield: 0.115 g (75%). Layering of a CH_2Cl_2 solution of the product with hexanes followed by cooling of this mixture to −30 °C afforded dark-red cubic single crystals after several days. ^{1}H NMR (CD_2Cl_2): δ 2.41 (m, 2H, SCH_2), 2.18 (m, 1H, CH_2), 2.11 (m, 2H, SCH_2), 1.76 (d, J_{P-H} = 8.9 Hz, 9H, PMe_3), 1.71 (m, 1H, CH_2), 1.60 (s, 18H, PMe_3). ^{31}P NMR (CD_2Cl_2): (20 °C) δ 20.8 (s, 1P, $Fe(CO)_2(PMe_3)$), 6.4 (s, 2P, $Fe(PMe_3)_2(NO)$); (−40 °C) δ 20.8 (s, 1P, $Fe(CO)_2(PMe_3)$), 7.5 (s, 2P, $Fe(PMe_3)_2(NO)$). IR (CH_2Cl_2): ν_{CO} = 1991, 1939 cm^{-1}; ν_{NO} = 1755 cm^{-1}. ESI-MS: *m*/*z* 532.3 (M^+). Anal. Calcd (Found) for $C_{14}H_{33}BF_4Fe_2NO_3P_3S_2$: C, 27.17 (27.26); H, 4.24 (5.67); N, 2.26 (2.48). CV (CH_2Cl_2, vs Ag|AgCl): E_{pc} = −0.93, −1.49 V; E_{pa} = 1.02, 1.20 V (reductions and oxidations were irreversible). During the synthesis of **3′**, in situ IR spectra (ReactIR 4000, Mettler Toledo; CH_2Cl_2): (−80 °C) ν_{CO} = 2034 and 1984 cm^{-1}, ν_{NO} = 1486 cm^{-1}; (−45 °C) ν_{CO} = 1953 cm^{-1}, $\nu_{\mu\text{-CO}}$ = 1984 cm^{-1}, ν_{NO} = 1760 cm^{-1}.

CO Binding Experiments. In a typical experiment, 0.7 mL of CD_2Cl_2 was distilled onto ∼8 mg of the diiron complex in a J. Young NMR tube, and the solution was frozen in an isopentane/N_2 bath and the tube evacuated. The tube was then pressurized with 1 atm of CO. After it was cooled to the appropriate temperature within the spectrometer, the reaction mixture was allowed to equilibrate until no significant changes were observed (typically ∼30−60 min). The probe temperature was calibrated with a methanol standard.

[2′CO]BF_4. ^{31}P NMR (CD_2Cl_2, −80 °C): δ 21.2 (s, 1P). IR (CH_2Cl_2, −80 °C): ν_{CO} = 2038, 2003 cm^{-1}; ν_{NO} = 1513 cm^{-1}.

[2CO]BF_4. ^{31}P NMR (CD_2Cl_2, −80 °C): δ 22.1 (s, 1P). IR (CH_2Cl_2, −80 °C): ν_{CO} = 2038, 2011, 1999 cm^{-1}; ν_{NO} = 1498 cm^{-1}.

[3′CO]BF_4. ^{31}P NMR (CD_2Cl_2, −80 °C): δ 19.5 (s, 1P), 19.3 (s, 1P), 18.2 (s, 1P), 18.1 (s, 2P), 17.5 (s, 1P). The low-temperature ^{31}P NMR spectrum indicated that [**3′**CO]BF_4 consists of two isomers, one containing three inequivalent phosphines and the other containing two equivalent and one inequivalent phosphine.

Isotopic Labeling Experiments. J. Young NMR tubes were pressurized to ∼0.3 atm of ^{13}CO, sealed, thawed in a CH_2Cl_2/N_2 slush bath, and then immediately transferred to a spectrometer, where the probe was cooled to the appropriate temperature. A series of spectra were collected and contained some combination of the following ^{13}C NMR (CD_2Cl_2, −80 °C) peaks: δ 222.2 (d, J_{C-P} = 25.1 Hz, **2′**), 211.3 (d, J_{C-P} = 12.0 Hz, **2′**), 210.8 (d, J_{C-P} = 10.4 Hz, **2′**$(CO)_{ap}$), 205.9 (d, J_{C-P} = 20.7 Hz, **2′**), 203.3 (d, J_{C-P} = 16.5 Hz, **2′**$(CO)_{ba}$). In particular:

1. The initial spectrum at −80 °C showed a doublet at δ 210.8 and a weak signal at δ 205.9.
2. The sample was then warmed briefly by ejecting it and then after 5 s reinjecting it into the −80 °C probe. The resulting spectrum showed signals of comparable intensity at δ 210.8 and 205.9.
3. The sample was then ejected, warmed at 20 °C for ∼5 min, and reinserted into the −80 °C probe; the resulting spectrum featured all five signals listed above.
4. (a) The sample was ejected, warmed to 20 °C for 5 min, and then vented to air. After the sample was cooled back to −80 °C, the spectrum showed peaks at δ 222.2, 211.3, and 205.9. (b) Alternatively, the sample was subjected to several freeze/pump/thaw cycles using a CH_2Cl_2/N_2 slush bath. The spectrum at −80 °C then consisted of a major signal at δ 205.9 and weaker signals at δ 222.2 and 211.3.

DNMR Measurements. With peaks at −30 °C labeled from left to right as A, B, C, and D, coalescence of peaks A and C occurred at $T_c \approx$ 10 °C with $\Delta\nu$ = 560 Hz, while coalescence of peaks B and D occurred at $T_c \approx$ 25 °C with $\Delta\nu$ = 2700 Hz. Substituting these values into eqs 3 and 4 yielded free energies of activation of 51.4 and 52.4 kJ/mol, respectively.[52]

$$k_c = \pi\Delta\nu/2^{1/2} \tag{3}$$

$$\Delta G^{\ddagger} = 19.14T_c[10.32 + \log(T_c/k_c)] \tag{4}$$

X-ray Powder Diffraction. Powder diffraction patterns for **2^{ap}** and **2^{ba}** were calculated from the single-crystal data using Topas, version 3, by Bruker AXS.

DFT Calculations. DFT calculations were carried out using the BP86 functional[53] and a valence triple-ζ basis set with polarization on all atoms (TZVP),[54] a level of theory which has been found to give reliable results for analogous organometallic compounds.[55]

(51) Mocella, M. T.; Okamoto, M. S.; Barefield, E. K. *Synth. React. Inorg. Met.-Org. Chem.* **1974**, *4*, 69–90.
(52) Nelson, J. H. *Nuclear Magnetic Resonance Spectroscopy*; Prentice Hall: New York, 2003.
(53) (a) Becke, A. D. *Phys. Rev. A* **1986**, *38*, 3098–3100. (b) Perdew, J. P. *Phys. Rev. B* **1986**, *33*, 8822–8824.

Stationary points on the energy hypersurface were located by means of energy-gradient techniques and a full vibrational analysis was carried out to further characterize each stationary point. Partial atomic charges were computed according to the NBO scheme.[56]

(54) Schaefer, A.; Huber, C.; Ahlrichs, R. *J. Chem. Phys.* **1994**, *100*, 5829–5835.
(55) (a) Niu, S.; Hall, M. B. *Chem. Rev* **2000**, *100*, 353–406. (b) Bruschi, M.; Zampella, G.; Fantucci, P.; De Gioia, L. *Coord. Chem. Rev.* **2005**, *249*, 1620–1640. (c) Siegbahn, P. E. M.; Tye, J. W.; Hall, M. B. *Chem. Rev.* **2007**, *107*, 4414–4435.
(56) Reed, A. E.; Weinstock, R. B.; Weinhold, F. *J. Chem. Phys.* **1985**, *83*, 735–746.

Acknowledgment. This research was supported by the National Institutes of Health and the Petroleum Research Fund. M.T.O. thanks the NIH Chemistry−Biology Interface program for support.

Supporting Information Available: Spectra, powder diffraction patterns, X-ray structures, voltammograms, DFT results, and crystal structure data in CIF format. This material is available free of charge via the Internet at http://pubs.acs.org.

JA802268P